G&M3D 1.0: an Interactive Framework for 3D Model Construction and Forward Calculation of Potential Fields

Dengkang Wang[1], Bo Chen[1,2,3], Kanggui Wei[4], Jiaxiang Peng[1] and Rongwen Guo[1,2,3]

[1]School of Geosciences and Info-Physics, Central South University, Changsha 410083, China
[2]Hunan Key Laboratory of Non-ferrous Resources and Geological Hazard Detection, Changsha 410083, China
[3]Key Laboratory of Metallogenic Prediction of Nonferrous Metals and Geological Environment Monitoring (Central South University), Ministry of Education, Changsha 410083, China
[4]Engineering Laboratory for Deep Resources Equipment and Technology, Institute of Geology and Geophysics, Beijing 100049, China

Correspondence to: Bo Chen (bochen@csu.edu.cn)

Abstract. Building source models and performing forward calculations are fundamental for processing, analyzing, and interpreting geophysical data. However, open-source tools that allow for both the flexible and interactive construction of source models and potential-field forward calculations are rare. To address this gap, we develop a new Qt-based software called G&M3D 1.0 (Gravity and Magnetic 3D modelling), which supports interactive three-dimensional (3D) model construction and provides accurate and efficient forward modelling. G&M3D 1.0 features two core functionalities: (1) constructing 3D gravity and magnetic source models and (2) calculating and visualizing their gravity/magnetic fields, as well as their gradient fields. In the 3D Modelling Module, user-defined anomalous bodies are internally discretized into assemblies of rectangular prisms for forward calculation. Based on this prism-based representation, users can conveniently construct regular bodies, such as spheres, cuboids, cylinders, ellipsoids and prismoids, and assign density contrast or magnetic parameters to them. Complex structures can be represented using the Irregular (Layer-Building) tool, which is especially suitable for stratigraphic or faulted formations. In addition, the Forward-Modelling Module allows for the rapid calculation, visualization, and saving of gravity anomalies, gravity gradients, total magnetic intensity, and magnetic gradients generated by the created 3D sources. To enhance computational efficiency, the software employs a 2D discrete convolution algorithm for the gravity and magnetic forward calculations. G&M3D 1.0 offers several significant advantages, including open-source accessibility, flexible interactive operations, an intuitive 3D modelling interface, efficient forward computation, and excellent file portability. As a demonstration of its capabilities, we use G&M3D 1.0 for forward gravity modelling over a salt dome at Vinton Dome in southern Louisiana, U.S., validating its accuracy and practicality.

1 Introduction

Compared with more logistically demanding methods, such as seismic reflection surveys and electrical surveys requiring dense electrode deployment, gravity and magnetic surveys generally offer simpler field procedures, lower acquisition costs, and greater efficiency for large-area data collection. Building forward source models and conducting forward calculations are fundamental to the processing, analysis, and interpretation of gravity and magnetic data (Blakely, 1996). Although several open-source tools already exist, few available tools combine interactive 3D body construction, gravity and magnetic forward calculation, and result visualization within a standalone graphical user interface (GUI).

To estimate the gravitational or magnetic effects generated by anomalous masses, geophysicists often represent complex subsurface volumes or geological bodies as a combination of idealized sources with simple shapes (Blakely, 1996; Hinze et al., 2013). These shapes include spheres, cylinders, vertical laminas, horizontal laminas, prisms, and polyhedra. Most of these idealized sources can be easily integrated over the volume and evaluated in closed analytical forms. Among these simple cells, the rectangular prism is particularly favoured for forward modelling and is also widely used in inversion studies, as it provides a straightforward way to approximate complicated anomalous sources and represents the total underground volume without

gaps (Caratori Tontini et al., 2009; Li and Chouteau, 1998; Zhao et al., 2018).

Numerous early scholars have contributed to the closed formulas for gravity and magnetic anomalies caused by rectangular prisms (Bhattacharyya, 1964; Bhattacharyya and Navolio, 1976; Li and Chouteau, 1998; Nagy, 1966; Nagy et al., 2000; Okabe, 1979; Plouff, 1976). For example, Bhattacharyya (1964) presented formulas for the magnetic anomalies resulting from prism-shaped bodies with arbitrary polarization. Nagy (1966) derived a closed expression to calculate the gravitational attraction of a rectangular prism. Bhattacharyya and Navolio (1976) provided spectral expressions for the gravity and magnetic anomalies arising from irregular three-dimensional (3D) sources by combining prisms. Later, Guo et al. (2004) introduced a new singularity-free calculation formula for the forward modelling of the magnetic field produced by a rectangular prism. Additionally, Luo and Yao (2007) optimized the theoretical magnetic calculation formula to enhance its computational efficiency.

A fine subdivision is often required to approximate anomalous bodies more precisely. However, when the subspace is finely subdivided, the repeated cumulative calculations can make the forward analysis time-consuming. To improve calculation efficiency, various algorithms have been developed for forward calculations of gravity and magnetic anomalies. For instance, Wu and Tian (2014) proposed a Gauss-fast Fourier transform (FFT) method for calculating potential fields in the Fourier domain. Zhang and Wong (2015) established a block-Toeplitz-Toeplitz-block (BTTB) structure using a discrete multi-layer model, then embedded the BTTB matrix into a block-cyclic-cyclic-block (BCCB) matrix by applying FFT in forward calculations. Additionally, Chen and Liu (2019) optimized the computation of the weight coefficient matrix and applied a 2D discrete convolution algorithm through block circulant extension (referred to as the BCE method) to calculate the gravity anomaly in the spatial domain. This method was later extended to calculate magnetic anomalies on undulating terrain (Qiang et al., 2019). Subsequently, Hogue et al. (2020) developed an open-source MATLAB code for evaluating gravity and magnetic kernels based on the BCE method. Recently, Yuan et al. (2022) advanced the BCE algorithm for magnetic forward modelling. Significant progress has been made in the forward calculation of the potential fields; however, constructing 3D anomalous models for algorithm testing or generating synthetic models for inversion studies remains complex and non-intuitive, especially when creating intricate, irregular sources (Jessell et al., 2021). To address these needs, various software packages have been developed for the computational synthesis of geological models and geophysical simulations (Bauville and Baumann, 2019; Cockett et al., 2015; de la Varga et al., 2019; Hassanzadeh et al., 2022; Pirot et al., 2022; Ulug and Karslıoglu, 2022; Wellmann et al., 2016). For example, SimPEG provides a flexible open-source framework for geophysical simulation (Cockett et al., 2015), while geomIO supports geometrical model construction for numerical simulations (Bauville and Baumann, 2019). Additionally, Hogue et al. (2020) developed open-source MATLAB code for the efficient evaluation of gravity and magnetic kernels, and SRBF_Soft focuses on regional gravity field modelling using spherical radial basis functions (Ulug and Karslıoglu, 2022). Despite these advancements, open-source options that seamlessly integrate interactive 3D body construction with efficient forward calculations within a standalone GUI remain rare. This study, therefore, aims to develop a free and open-source software framework that bridges this gap by integrating flexible model construction with high-performance forward calculation of potential fields.

C++ is a widely used general-purpose programming language with strong computational performance and portability, making it well suited for numerical computing and scientific software development. Qt (https://wiki.qt.io), a powerful cross-platform C++ framework, is widely used for designing GUI applications across various platforms, including desktop, mobile, and embedded systems. It offers extensive development tools and libraries that facilitate the rapid creation of high-quality applications. For instance, Snopek and Casten (2006) developed the 3GRAINS software using standard C++ with the Qt library for gravity data interpretation.

In this study, we choose the rectangular prism as the primary cell to approximate the source volume. We then develop a software package called G&M3D 1.0 to construct 3D density contrast and magnetization models, as well as to perform forward calculations and visualize their gravity and magnetic fields using the Qt Creator framework and C++. The software includes

the following functions: (1) interactively creating various geological models and assigning density contrasts or magnetization parameters; (2) performing fast and accurate forward calculations of gravity, gravity gradients, total magnetic intensity, and magnetic gradients. In addition, G&M3D 1.0 supports visualizing, saving, and exporting the constructed models and the corresponding density or magnetization distributions, as well as the forward-modelling results.

The paper is organized as follows. Section 2 introduces the principles of gravity and magnetic forward calculation, as well as fast calculation strategies. In section 3, we describe the software workflow, focusing on how to create a source model and conduct forward modelling. Section 4 presents an example of applying G&M3D 1.0 to the real-world forward gravity modelling at Vinton Dome, southern Louisiana, U.S. The final section is the conclusions.

2 Forward Method

2.1 Forward modelling theory

As shown in Figure 1, a collection of rectangular prisms offers a straightforward way to approximate the volume of an anomalous body (Li and Chouteau, 1998). Each prism is assumed to have constant physical properties, such as density contrast or magnetization. For a rectangular prism whose dimensions are constrained as $[\xi_1,\xi_2],[\eta_1,\eta_2],[\zeta_1,\zeta_2]$ in the x, y, and z directions (Figure 1), according to Li and Chouteau (1998) and Nagy et al. (2000), the vertical component of the gravity attraction Δg and the gravity gradient components V_{zz}, V_{xx}, V_{yy}, V_{xz}, V_{zx}, V_{yz}, V_{zy}, V_{xy} and V_{yx} at the observation point $P(x,y,z_0)$ are given by:

$$\Delta g(x,y,z_0) = -G\Delta\rho\sum_{i=1}^{2}\sum_{j=1}^{2}\sum_{k=1}^{2}u_{ijk}\left[x_i\ln\left(r_{ijk}+y_j\right)+y_j\ln\left(r_{ijk}+x_i\right)-z_k\arctan\frac{x_i y_j}{z_k r_{ijk}}\right], \tag{1}$$

$$V_{zz}(x,y,z_0) = G\Delta\rho\sum_{i=1}^{2}\sum_{j=1}^{2}\sum_{k=1}^{2}u_{ijk}\arctan\frac{x_i y_j}{z_k r_{ijk}}, \tag{2}$$

$$V_{xx}(x,y,z_0) = G\Delta\rho\sum_{i=1}^{2}\sum_{j=1}^{2}\sum_{k=1}^{2}u_{ijk}\arctan\frac{y_j z_k}{x_i r_{ijk}}, \tag{3}$$

$$V_{yy}(x,y,z_0) = G\Delta\rho\sum_{i=1}^{2}\sum_{j=1}^{2}\sum_{k=1}^{2}u_{ijk}\arctan\frac{x_i z_k}{y_j r_{ijk}}, \tag{4}$$

$$V_{xz}(x,y,z_0) = V_{zx}(x,y,z_0) = -G\Delta\rho\sum_{i=1}^{2}\sum_{j=1}^{2}\sum_{k=1}^{2}u_{ijk}\ln\left(r_{ijk}+y_j\right), \tag{5}$$

$$V_{yz}(x,y,z_0) = V_{zy}(x,y,z_0) = -G\Delta\rho\sum_{i=1}^{2}\sum_{j=1}^{2}\sum_{k=1}^{2}u_{ijk}\ln\left(r_{ijk}+x_i\right), \tag{6}$$

$$V_{xy}(x,y,z_0) = V_{yx}(x,y,z_0) = -G\Delta\rho\sum_{i=1}^{2}\sum_{j=1}^{2}\sum_{k=1}^{2}u_{ijk}\ln\left(r_{ijk}+z_k\right), \tag{7}$$

where G is the universal gravitational constant ($6.672\times10^{-11}\,\mathrm{m^3kg^{-1}s^{-2}}$), $\Delta\rho$ is the density contrast of the rectangular prism, $x_i = x-\xi_i$, $y_j = y-\eta_j$, $z_k = z_0-\zeta_k$, $r_{ijk} = \sqrt{x_i^2+y_j^2+z_k^2}$, and $u_{ijk} = (-1)^i(-1)^j(-1)^k$. The z-axis is taken to be positive downward.

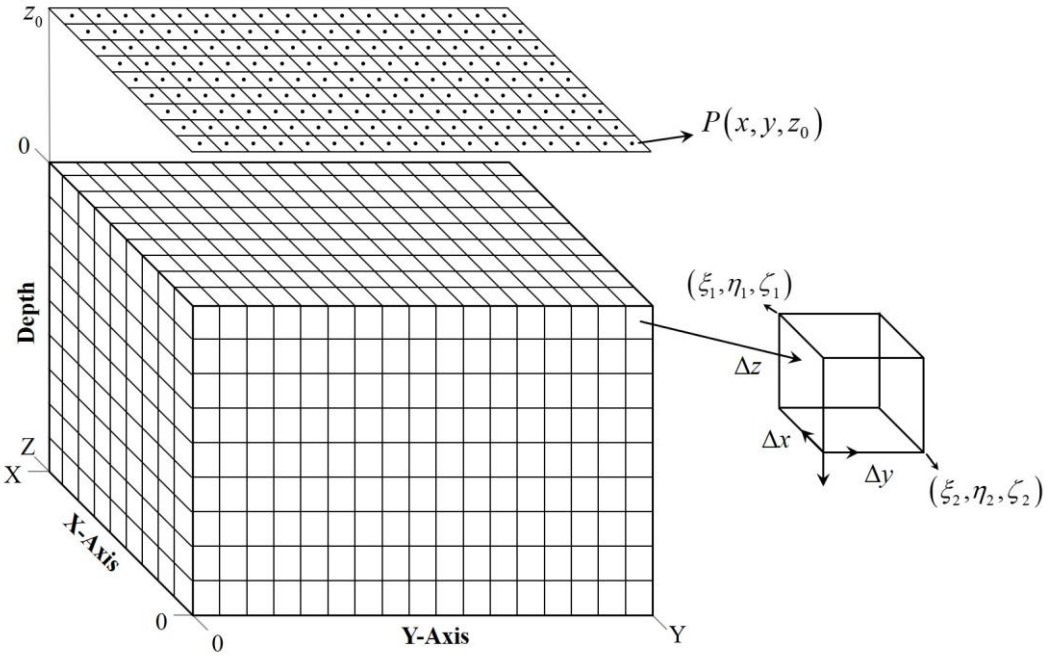

Figure 1: Division schematic diagram of the source region and observation points.

According to Luo and Yao (2007), the three components of the magnetic field anomaly (B_x, B_y, B_z) and its gradient tensors due to the prism at the observation point $P(x, y, z_0)$ are given by:

$$B_x(x,y,z_0) = \frac{\mu_0 M}{4\pi}\sum_{i=1}^{2}\sum_{j=1}^{2}\sum_{k=1}^{2} u_{ijk}\left[-k_1 \arctan\frac{y_j z_k}{x_i r_{ijk}} + k_2 \ln\left(r_{ijk}+z_k\right) + k_3 \ln\left(r_{ijk}+y_j\right)\right], \tag{8}$$

$$B_y(x,y,z_0) = \frac{\mu_0 M}{4\pi}\sum_{i=1}^{2}\sum_{j=1}^{2}\sum_{k=1}^{2} u_{ijk}\left[k_1 \ln\left(r_{ijk}+z_k\right) - k_2 \arctan\frac{x_i z_k}{y_j r_{ijk}} + k_3 \ln\left(r_{ijk}+x_i\right)\right], \tag{9}$$

$$B_z(x,y,z_0) = \frac{\mu_0 M}{4\pi}\sum_{i=1}^{2}\sum_{j=1}^{2}\sum_{k=1}^{2} u_{ijk}\left[k_1 \ln\left(r_{ijk}+y_j\right) + k_2 \ln\left(r_{ijk}+x_i\right) - k_3 \arctan\frac{x_i y_j}{z_k r_{ijk}}\right], \tag{10}$$

$$B_{xx}(x,y,z_0) = -\frac{\mu_0 M}{4\pi}\sum_{i=1}^{2}\sum_{j=1}^{2}\sum_{k=1}^{2} u_{ijk}\left[k_1 \frac{y_j z_k\left(r_{ijk}^2+x_i^2\right)}{\left(x_i^2+z_k^2\right)\left(x_i^2+y_j^2\right)r_{ijk}} + k_2 \frac{x_i}{r_{ijk}\left(r_{ijk}+z_k\right)} + k_3 \frac{x_i}{r_{ijk}\left(r_{ijk}+y_j\right)}\right], \tag{11}$$

$$B_{yy}(x,y,z_0) = -\frac{\mu_0 M}{4\pi}\sum_{i=1}^{2}\sum_{j=1}^{2}\sum_{k=1}^{2} u_{ijk}\left[k_1 \frac{y_j}{r_{ijk}\left(r_{ijk}+z_k\right)} + k_2 \frac{x_i z_k\left(r_{ijk}^2+y_j^2\right)}{\left(y_j^2+z_k^2\right)\left(x_i^2+y_j^2\right)r_{ijk}} + k_3 \frac{y_j}{r_{ijk}\left(r_{ijk}+x_i\right)}\right], \tag{12}$$

$$B_{zz}(x,y,z_0) = -\frac{\mu_0 M}{4\pi}\sum_{i=1}^{2}\sum_{j=1}^{2}\sum_{k=1}^{2} u_{ijk}\left[k_1 \frac{z_k}{r_{ijk}\left(r_{ijk}+y_j\right)} + k_2 \frac{z_k}{r_{ijk}\left(r_{ijk}+x_i\right)} + k_3 \frac{x_i y_j\left(r_{ijk}^2+z_k^2\right)}{\left(x_i^2+z_k^2\right)\left(y_j^2+z_k^2\right)r_{ijk}}\right], \tag{13}$$

$$B_{xy}(x,y,z_0) = B_{yx}(x,y,z_0) = -\frac{\mu_0 M}{4\pi}\sum_{i=1}^{2}\sum_{j=1}^{2}\sum_{k=1}^{2} u_{ijk}\left[k_1 \frac{x_i}{r_{ijk}\left(r_{ijk}+z_k\right)} + k_2 \frac{y_j}{r_{ijk}\left(r_{ijk}+z_k\right)} + k_3 \frac{1}{r_{ijk}}\right], \tag{14}$$

$$B_{yz}(x,y,z_0) = B_{zy}(x,y,z_0) = -\frac{\mu_0 M}{4\pi}\sum_{i=1}^{2}\sum_{j=1}^{2}\sum_{k=1}^{2} u_{ijk}\left[k_1 \frac{1}{r_{ijk}} + k_2 \frac{y_j}{r_{ijk}\left(r_{ijk}+x_i\right)} + k_3 \frac{z_k}{r_{ijk}\left(r_{ijk}+x_i\right)}\right], \tag{15}$$

$$B_{xz}(x,y,z_0) = B_{zx}(x,y,z_0) = -\frac{\mu_0 M}{4\pi}\sum_{i=1}^{2}\sum_{j=1}^{2}\sum_{k=1}^{2} u_{ijk}\left[k_1 \frac{x_i}{r_{ijk}\left(r_{ijk}+y_j\right)} + k_2 \frac{1}{r_{ijk}} + k_3 \frac{z_k}{r_{ijk}\left(r_{ijk}+y_j\right)}\right], \tag{16}$$

where M is the induced magnetization intensity of the rectangular prism with the inclination (I') and declination (D'), $k_1 = \cos I' \cos D'$, $k_2 = \cos I' \sin D'$, $k_3 = \sin I'$, $\mu_0 = 4\pi \times 10^{-7}\ \mathrm{H \cdot m^{-1}}$ is the magnetic permeability of the vacuum.

Suppose the magnetic anomaly caused by a magnetic body is small compared with the Earth's main magnetic field. Then the scalar magnitude of the magnetic field anomalies can be approximately calculated by projecting the components of the anomalous field in the direction of the Earth's main magnetic field (Hinze et al., 2013; Plouff, 1976). As a result, the total magnetic intensity anomaly ΔT and its gradients $(\Delta T_x, \Delta T_y, \Delta T_z)$ from the source can be approximated by:

$$\Delta T = B_x \cos I \cos D + B_y \cos I \sin D + B_z \sin I, \tag{17}$$

$$\Delta T_x = B_{xx} \cos I \cos D + B_{yx} \cos I \sin D + B_{zx} \sin I, \tag{18}$$

$$\Delta T_y = B_{xy} \cos I \cos D + B_{yy} \cos I \sin D + B_{zy} \sin I, \tag{19}$$

$$\Delta T_z = B_{xz} \cos I \cos D + B_{yz} \cos I \sin D + B_{zz} \sin I, \tag{20}$$

where I and D are the inclination and declination of the Earth's geomagnetic field at the observation point.

2.2 Fast forward modelling method

In G&M3D 1.0, we define a source region with the range $[0, X]$, $[0, Y]$, and $[0, Z]$ in the x, y, and z axes, respectively. The source space is divided into $N \times M \times L$ prisms, each with dimensions of $\Delta x \times \Delta y \times \Delta z$. These prisms are labeled as (a, b, c), with their dimensions limited to $[\xi_{1,a} = (a-1)\Delta x, \xi_{2,a} = a\Delta x]$, $[\eta_{1,b} = (b-1)\Delta y, \eta_{2,b} = b\Delta y]$, $[\zeta_{1,c} = (c-1)\Delta z, \zeta_{2,c} = c\Delta z]$, where $a = 1, 2, \cdots, N$; $b = 1, 2, \cdots, M$; $c = 1, 2, \cdots, L$.

The observation points $P(x_n, y_m, z_0)$, where $x_n = (n - 0.5)\Delta x$, $n = 1, \cdots, N$, $y_m = (m - 0.5)\Delta y$, $m = 1, \cdots, M$, are distributed at the horizontal surface z_0 at regular intervals, aligned with the prism centers, as shown in Figure 1. The gravity/magnetic fields at the observation point $P(x_n, y_m, z_0)$ can be calculated by summing the contributions from all prisms within the source region:

$$g(x_n, y_m, z_0) = \sum_{c=1}^{L} \left[\sum_{a=1}^{N} \sum_{b=1}^{M} f(a, b, c) \times t(x_n, y_m, z_0, a, b, c) \right], \tag{21}$$

where $f(a, b, c)$ is the density contrast or magnetization value corresponding to the prism (a, b, c), and $t(x_n, y_m, z_0, a, b, c)$ is the field response at $P(x_n, y_m, z_0)$ generated by prism (a, b, c) with unit density contrast or magnetization. Therefore, t represents the kernel (or sensitivity) coefficient, which can be evaluated using any of Eqs. (1) to (16), rather than a simple distance-dependent decay term.

Thanks to Eq. (21), the gravity/magnetic field at all observation points can be presented in matrix-vector form as follows,

$$\mathbf{g} = \mathbf{K} \cdot \mathbf{f}, \tag{22}$$

where $\mathbf{g}$ is the field vector, $\mathbf{f}$ is the density contrast or magnetization parameter vector, $\mathbf{K}$ represents the kernel matrix (or sensitivity matrix) with dimension $(N \times M) \times (N \times M \times L)$, which is classified as a Block-Toeplitz Toeplitz-Block (BTTB) matrix.

The forward calculations described in Eq. (22) can be time-consuming, particularly when the source space is large and finely discretized. In this study, we apply a 2D discrete convolution algorithm using block circulant extension (BCE) (Chen and Liu, 2019) to optimize the forward calculations. In G&M3D 1.0, we conduct forward calculations of potential fields layer by layer along the z direction using the BCE algorithm. The procedure for the BCE algorithm (Chen and Liu, 2019) is as follows.

First, the density contrast or magnetization values of all the prisms are stored in a 3D matrix $\mathbf{E}$ of size $N \times M \times L$. For any given layer (e.g., the c^{th} layer, $c = 1, \cdots, L$), the parameter vector is defined as $\mathbf{f} = \mathbf{E}(1{:}N, 1{:}M, c)$. A null parameter vector $\mathbf{f}$ (where all elements equal zero) indicates that the prisms in the c^{th} layer make no contribution to the observed field. For non-zero cases, the matrix $\mathbf{f}$ is extended with zeros to form an extended parameter matrix $\mathbf{F}$,

$$\mathbf{F}=\begin{bmatrix}\mathbf{f} & \mathbf{0}_{N\times M}\\ \mathbf{0}_{N\times M} & \mathbf{0}_{N\times M}\end{bmatrix}. \tag{23}$$

Next, to implement the BCE-based discrete convolution, the observation range is extended along the negative directions of the x-axis and y-axis from $[0,X]$, $[0,Y]$ to $[-X+\Delta x,X]$, $[-Y+\Delta y,Y]$, as shown in Figure 2. This extension is necessary because Eq. (21) represents a linear convolution, whereas the FFT inherently evaluates a circular convolution. By embedding the original problem into an extended domain, the linear convolution can be reformulated in a circulant form and computed efficiently without introducing wrap-around boundary errors at the boundaries. We then compute the field effects generated by the prism $(a=1,b=1,c)$ (dimensions limited as $[\xi_1=0,\xi_2=\Delta x]$, $[\eta_1=0,\eta_2=\Delta y]$, $[\zeta_1=(c-1)\Delta z,\zeta_2=c\Delta z]$) at all observation points in the extended area. Note that the extended area serves only as an auxiliary computational domain; only the results within the original observation region are retained. This results in an extended response matrix $\mathbf{T}$ with a size of $(2N-1)\times(2M-1)$ for the c^{th} layer,

$$\mathbf{T}=\begin{bmatrix}t_{1,1} & \cdots & t_{1,2M-1}\\ \vdots & t_{n',m'} & \vdots\\ t_{2N-1,1} & \cdots & t_{2N-1,2M-1}\end{bmatrix}, \tag{24}$$

where $t_{n',m'}\,(n'=1,2,\cdots,2N-1;\,m'=1,2,\cdots,2M-1)$ is the field response at the observation $P(x_n,y_m,z_0)$ where $x_{n'}=(n'-N+0.5)\Delta x$, $y_{m'}=(m'-M+0.5)\Delta y$, which is calculated using Eqs. (1) to (16) with unit density contrast or induced magnetization intensity (namely, $\Delta\rho=1$, $M=1$).

We extend $\mathbf{T}$ by zeros along the top and the left margins, as shown in Figure 2. This creates a matrix $\mathbf{T}_0$ with a size of $2N\times 2M$,

$$\mathbf{T}_0=\begin{bmatrix}0 & \mathbf{0}_{1\times(2M-1)}\\ \mathbf{0}_{(2N-1)\times 1} & \mathbf{T}\end{bmatrix}, \tag{25}$$

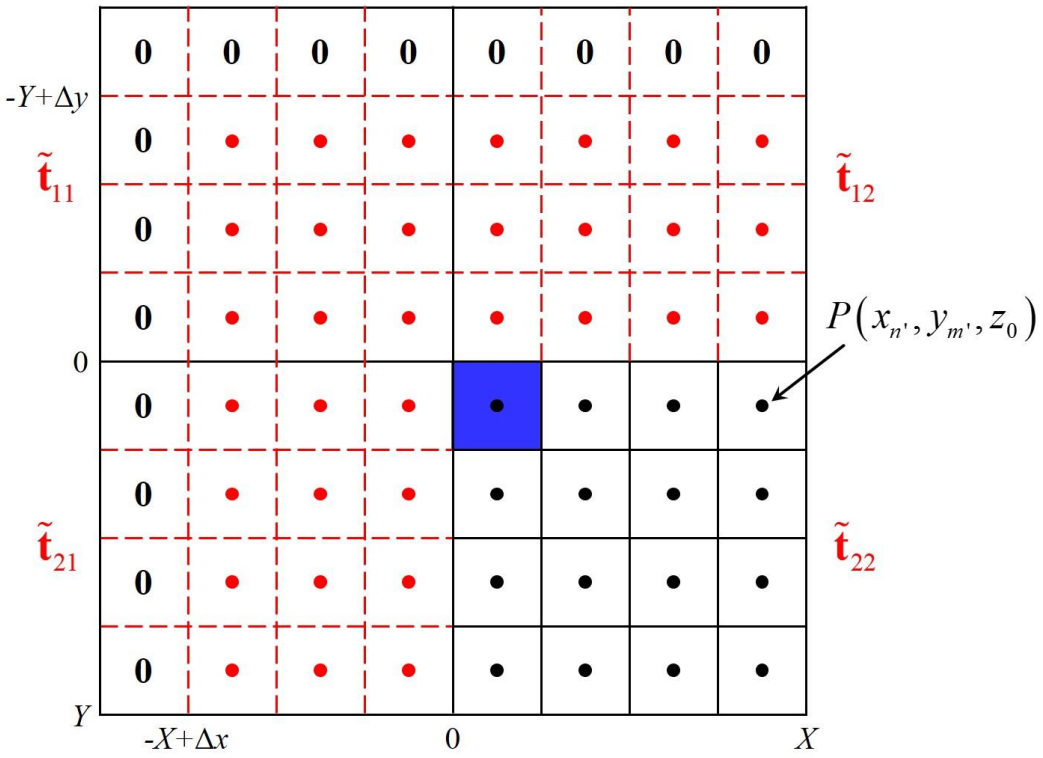

Figure 2: The sketch map shows the extended observation points and source region for the BCE method. The extended observation points are shown in red, and the observation points in the original observation domain are shown in black. The prism (1, 1) is marked in blue. A single-layer model consisting of 4×4 prisms is taken as an example.

The matrix $\mathbf{T}_0$ in Eq. (25) can then be rewritten into four $N \times M$ submatrices as,

$$\mathbf{T}_0 = \begin{bmatrix} \tilde{\mathbf{t}}_{11} & \tilde{\mathbf{t}}_{12} \\ \tilde{\mathbf{t}}_{21} & \tilde{\mathbf{t}}_{22} \end{bmatrix}. \tag{26}$$

By reordering the submatrices in Eq. (24), we get

$$\mathbf{C} = \begin{bmatrix} \tilde{\mathbf{t}}_{22} & \tilde{\mathbf{t}}_{21} \\ \tilde{\mathbf{t}}_{12} & \tilde{\mathbf{t}}_{11} \end{bmatrix}. \tag{27}$$

The matrix $\mathbf{C}$ in Eq. (27) is identified as a Block-Cyclic-Cyclic-Block (BCCB) matrix. The 2D discrete convolution of this matrix with the extended parameter matrix $\mathbf{F}$ can be efficiently computed using the fast Fourier transform (Chen and Liu, 2019; Vogel, 2002) as follows,

$$\tilde{\mathbf{C}} = fft2(\mathbf{C}), \tag{28}$$

$$\tilde{\mathbf{F}} = fft2(\mathbf{F}), \tag{29}$$

$$\tilde{\mathbf{G}} = \tilde{\mathbf{C}} .* \tilde{\mathbf{F}}, \tag{30}$$

$$\mathbf{G} = ifft2\left(\tilde{\mathbf{G}}\right), \tag{31}$$

$$\mathbf{G}_c = \mathbf{G}(1:N, 1:M), \tag{32}$$

where $fft2$ is the 2D fast Fourier transform, and $ifft2$ denotes the 2D inverse fast Fourier transform. The symbol $.*$ represents the dot multiplication operator. $\mathbf{G}_c$ is the resulting field at the observations generated by the anomalous prisms in the c^{th} layer.

Repeat these steps for each layer, and the total field $\mathbf{g}$ at all observations is obtained by,

$$\mathbf{g} = \sum_{c=1}^{L} \mathbf{G}_c, \tag{33}$$

From a programming perspective, we implement two strategies to enhance computational efficiency in G&M3D 1.0.

Strategy 1. We take advantage of the fast matrix operation in Qt to optimize the forward calculations in G&M3D 1.0. We construct in advance two new matrices $\mathbf{X}_i$ and $\mathbf{Y}_j$ with sizes of $(2N-1)\times(2M-1)$,

$$\mathbf{X}_i = \begin{bmatrix} x_1 & \cdots & x_1 \\ \vdots & x_{n'} & \vdots \\ x_{2N-1} & \cdots & x_{2N-1} \end{bmatrix} - \xi_i \mathbf{I}, \tag{34}$$

$$\mathbf{Y}_j = \begin{bmatrix} y_1 & \cdots & y_{2M-1} \\ \vdots & y_{m'} & \vdots \\ y_1 & \cdots & y_{2M-1} \end{bmatrix} - \eta_j \mathbf{I}, \tag{35}$$

where $i, j = 1, 2$, $x_{n'} = (n' - N + 0.5)\Delta x$, $y_{m'} = (m' - M + 0.5)\Delta y$, $(n' = 1, 2, \cdots, 2N-1;\ m' = 1, 2, \cdots, 2M-1)$, $\xi_1 = 0$, $\xi_2 = \Delta x$, $\eta_1 = 0$, $\eta_2 = \Delta y$. $\mathbf{I}$ is an all-ones matrix. Thanks to the Eqs. (32) to (33), we can substitute the matrices $\mathbf{X}_i$ and $\mathbf{Y}_j$ to x_i and y_j in any of the Eqs (1) to (16). This allows the extended response matrix $\mathbf{T}$ at all observations to be computed by a single dot product in Qt, rather than relying on a large number of cyclic calculations.

Strategy 2. Since the kernel matrices for gravity and magnetic components under vertical magnetization are symmetric (Hogue et al., 2020), k_1 and k_2 in Eqs. (8) to (16) are zero, and only k_3 remains. In these cases, we only calculate the submatrix $\tilde{\mathbf{t}}_{22}$ in $\mathbf{C}$ (Eq. (27)) for these cases. The other three submatrices $(\tilde{\mathbf{t}}_{11}, \tilde{\mathbf{t}}_{12}, \tilde{\mathbf{t}}_{21})$ can be derived from $\tilde{\mathbf{t}}_{22}$, because they share the same value or have the opposite sign as $\tilde{\mathbf{t}}_{22}$. This strategy results in a higher efficiency for forward calculations of gravity

anomalies, gravity gradient tensor, and magnetic components with vertical magnetization compared to those for the magnetic field with non-vertical magnetization. As we know, the forward calculations of magnetic fields depend on the declination and inclination of the sources. If the anomalous bodies in the source model have varying declinations or inclinations, we classify these bodies by their declinations or inclinations and perform forward calculations of each category separately.

2.3 Synthetic model tests

To verify the efficiency of the forward calculation in G&M3D 1.0, we design a synthetic model with specified density contrast and magnetization for gravity and magnetic forward calculations. The model region extends from 0 to 50 km along the x, y, and z axes. It consists of an anomalous body with a density contrast of $1\ \mathrm{g\cdot cm^{-3}}$ and an induced magnetization of $1\ \mathrm{A\cdot m^{-1}}$. The center of the body is located at (25, 25, 25) km with a size of $25 \times 25 \times 20\ \mathrm{km^3}$.

We evaluate the computation time for gravity and magnetic forward calculations at five different numerical resolutions, employing 50 × 50 × 50, 100 × 100 × 100, 200 × 200 × 200, 400 × 400 × 400, and 800 × 800 × 800 prisms in the x-, y-, and z-directions, respectively. This corresponds to grid intervals of 1000 m, 500 m, 250 m, 125 m, and 62.5 m. In these tests, the observation points are set at the horizontal positions corresponding to the prism centers. Consequently, as the numerical resolution increases, the number of observation points also grows accordingly. The absolute computation times for the forward calculation of the gravity and magnetic fields are summarized in Table 1.

Table 1: The statistics of the absolute consumption times for forward computations of the gravity and magnetic fields with five different numerical resolutions.

Grid interval (m) / Numerical resolutions	Values are reported as serial / parallel computation times (s)		
	Gravity components	Magnetic components for vertical magnetization	Magnetic components for non-vertical magnetization
1000.0 / 50 × 50 × 50	0.16 / 0.03	0.15 / 0.02	0.46 / 0.12
500.0 / 100 × 100 × 100	1.32 / 0.55	1.45 / 0.56	4.05 / 1.34
250.0 / 200 × 200 × 200	10.15 / 2.52	9.68 / 2.93	34.37 / 13.93
125.0 / 400 × 400 × 400	39.69 / 12.48	50.38 / 20.99	131.60 / 39.16
62.5 / 800 × 800 × 800	331.25 / 98.58	425.99 / 143.84	1119.36 / 433.86

Note. All the tests are carried out on a desktop with an AMD Ryzen 7 3700X CPU (8 cores) and 32 GB of memory.

Table 1 shows that the computation time increases significantly as the numerical resolution increases. Note that the output results of the gravity calculation in Table 1 consist of 7 components, i.e., Δg, V_{zz}, V_{xx}, V_{yy}, V_{xz}, V_{yz}, V_{xy}, and the results of magnetic forward modelling include 13 components (i.e., B_x, B_y, B_z, B_{xx}, B_{yy}, B_{zz}, B_{xy}, B_{xz}, B_{yz}, ΔT, ΔT_x, ΔT_y, ΔT_z). Due to the implementation of Strategy 2, which decouples the computation of vertically and non-vertically magnetized models, the efficiency of forward modelling improves significantly. In a 200 × 200 × 200 grid case, the computation time is reduced by 71.83% (34.37 s vs 9.68 s). These tests demonstrate that G&M3D 1.0 is a high-speed tool for forward calculations of the gravity and magnetic fields. It is worth noting that the layers with non-zero density/magnetization occupy 40% of the total layers in the z direction in these tests. The forward calculation is faster if the anomalous body's vertical dimension is reduced, but it requires more time if the vertical dimension increases. For example, in the 100 × 100 × 100 case, under vertical magnetization conditions, two anomalous bodies with the same number of non-zero prisms but different spatial distributions, namely 1 × 1 × 100 prisms and 100 × 1 × 1 prisms, require total computation times of about 2.65 s and 0.04 s, respectively, when calculating gravity anomalies, magnetic anomalies, and the corresponding gradient components.

To further enhance the computational performance, we implement parallel computation for the layer-by-layer forward calculations along the z-direction. In the BCE framework, the field contribution of each layer is computed independently, and the final response is obtained by summing the contributions from all layers. The parallelization is realized using task-based multithreading (standard C++), where layer-wise forward responses are launched asynchronously and collected after

completion. Using the same synthetic model, discretized into 200 × 200 × 200 prisms, we record the computation times under vertical magnetization conditions using 8 threads, and the computation is approximately 3.45 times faster than that of the serial implementation.

To evaluate G&M3D 1.0 against existing open-source tools, we compare its computational efficiency with SimPEG (Cockett et al., 2015). For the 200 × 200 × 200 case, the gravity forward calculation in SimPEG takes 1606.62 s, whereas G&M3D 1.0 requires only 2.52 s. Notably, at 800 × 800 × 800 resolution, SimPEG fails due to excessive memory overflow, while G&M3D 1.0 maintains robust performance.

To validate the computational accuracy of G&M3D 1.0, we design a synthetic model consisting of three buried spheres, for which analytical solutions are available. The centers of the three spheres are located at (50 m, 55 m, 50 m), (140 m, 75 m, 65 m), and (110 m, 155 m, 80 m), with radii of 20 m, 30 m, and 35 m, respectively. The density contrasts are all set to $1\ \mathrm{g\cdot cm^{-3}}$, and the induced magnetizations are all set to $1\ \mathrm{A\cdot m^{-1}}$. The computational domain is 200 m × 200 m × 200 m, which is discretized into 800 × 800 × 800 cells. Gravity anomalies Δg and magnetic anomalies ΔT are calculated separately, and the corresponding analytical solutions serve as references. The computed and analytical results are compared in Figure 3. As shown in Figure 3, the differences between our results and the analytical solutions are negligible. The maximum absolute errors of the gravity and magnetic anomalies are 7.5×10^{-6} mGal and 5.4×10^{-3} nT, respectively.

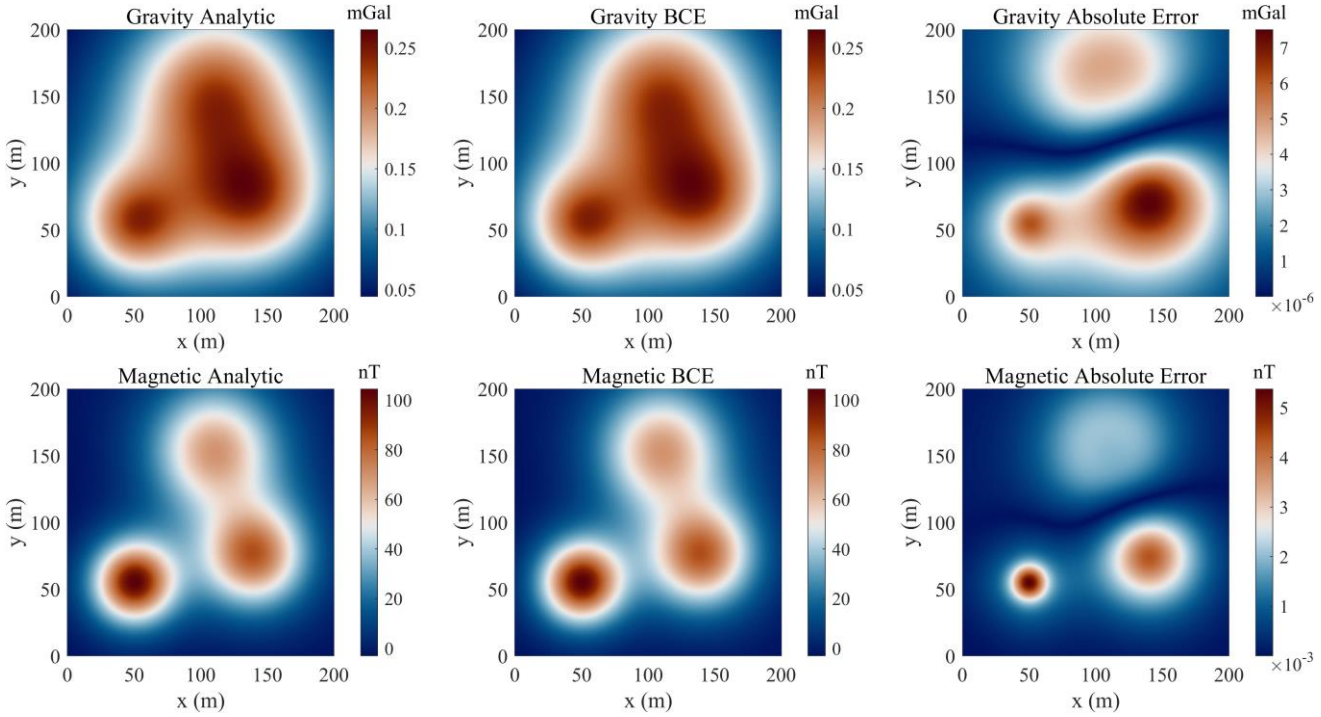

Figure 3: Comparison between analytical solutions and BCE results for gravity and magnetic anomalies produced by a synthetic model of three buried spheres.

3 The framework and functions of G&M3D

In this section, we introduce the functions and operational procedures of G&M3D 1.0. The software consists of two main modules: (1) a 3D-Modelling module for constructing source bodies and assigning physical properties, and (2) a Forward-Modelling module for calculating and visualizing the resulting gravity and magnetic fields. The workflow of G&M3D 1.0 is shown in Figure 4. Architecturally, G&M3D 1.0 separates interactive model construction from numerical forward computation, with model data serving as an intermediate layer between the GUI and the forward-calculation kernels, thereby enhancing maintainability and extensibility. In addition, the software supports topography modelling. Users can import and visualize a topographic surface, where anomalous bodies are constrained to remain below it, and observation points can be assigned topography-dependent elevations for forward calculations over non-planar observation surfaces.

G&M3D 1.0 is based on a right-handed Cartesian coordinate system. When users open G&M3D 1.0 and enter the start interface (Figure 4), they can access the 3D-Modelling module to create a new source model by clicking the button **Create Model**, or they can input an existing model data file to conduct gravity or magnetic forward calculations through the Forward-Modelling module by clicking the button **Input Model**.

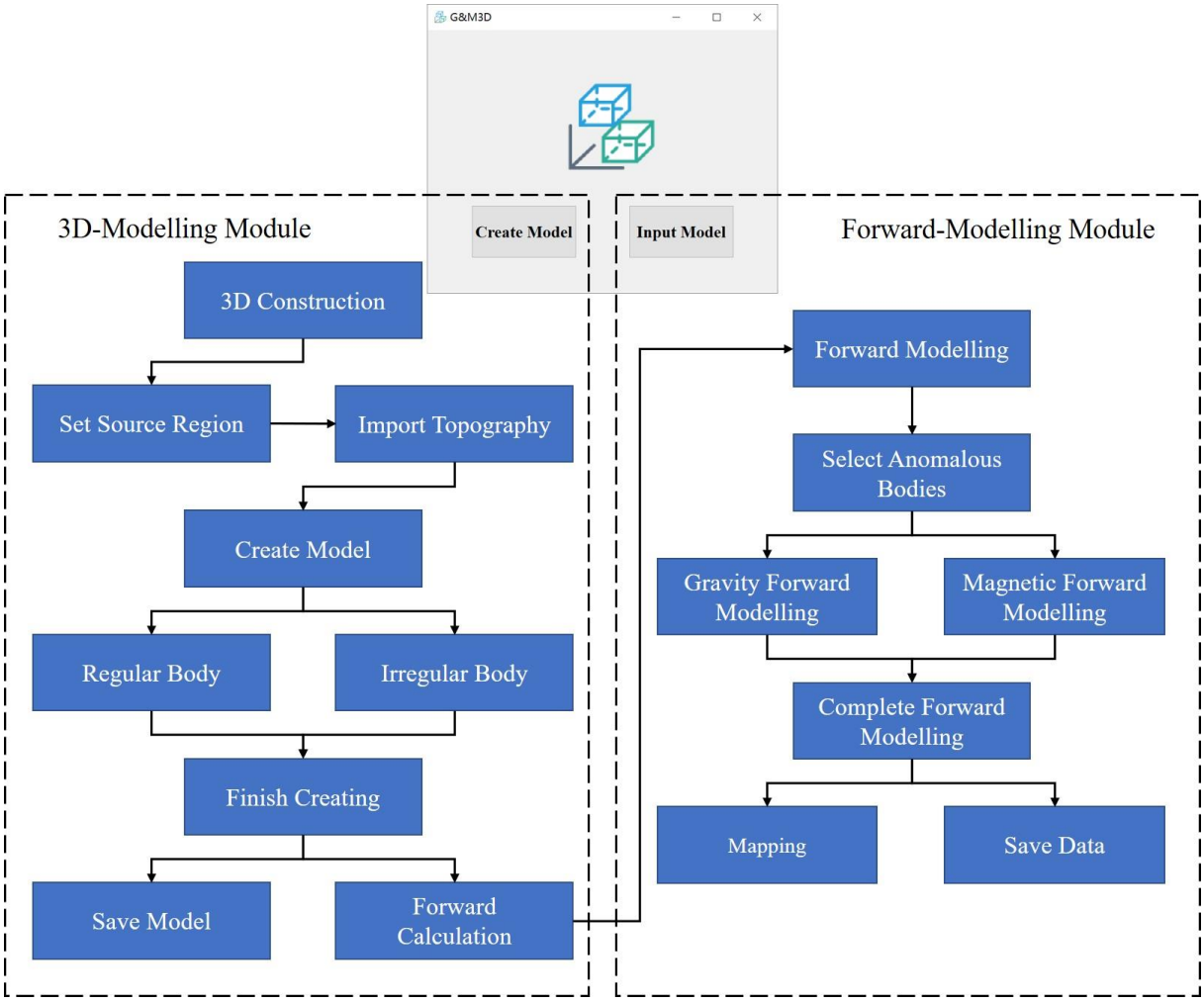

Figure 4: Workflow in G&M3D 1.0 and G&M3D 1.0 initial interface.

The main interface of the Modelling module is shown in Figure 5a. By default, G&M3D 1.0 generates an initial source region (Figure 5b). To customize this for their needs, users should first set the source region by clicking the "Settings" button in the operation area of the main interface. In the pop-up window for the Setting Field (Figure 5b), users can configure the basic parameters that define the source region, including the source range, mesh interval, and length unit. The supported length units are meters (m), hectometers (hm), and kilometers (km), which allow for multi-scale forward modelling simulations. If a topographic file is available, users should import it before model construction by using the "Import Topo" function in G&M3D 1.0.

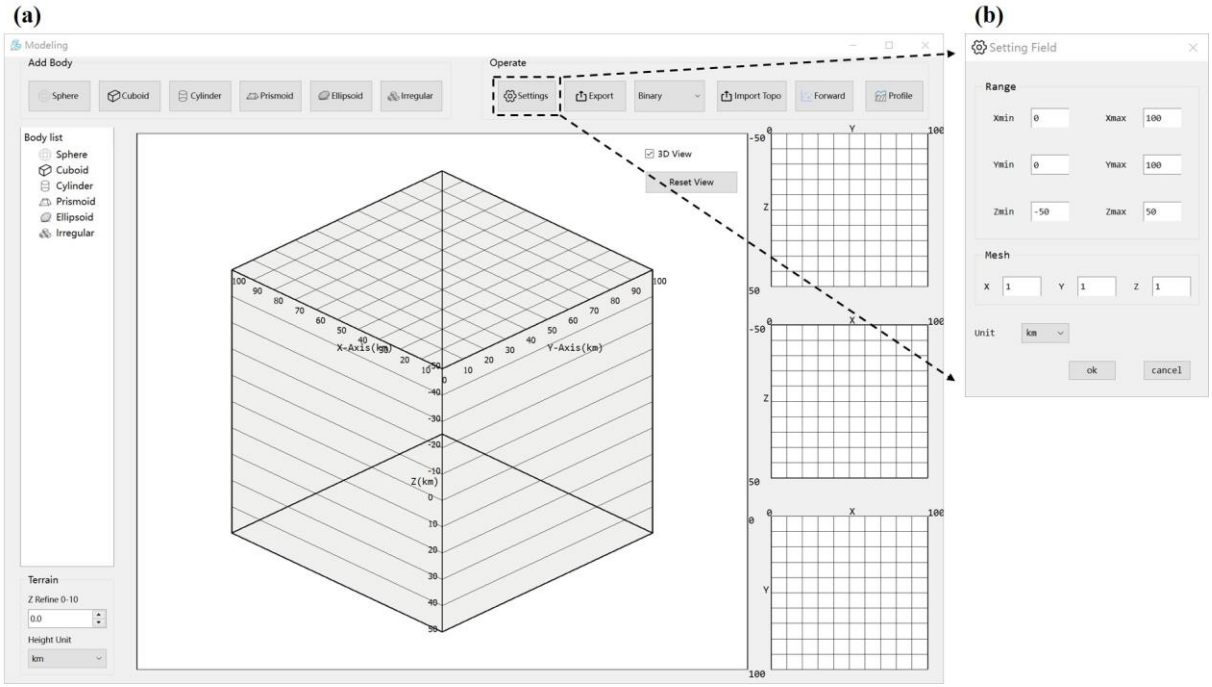

Figure 5: (a) Interface of the Modelling Module. The top functional area contains tools for creating different shapes on the left and various action buttons on the right. The middle workspace is used to display the created models (the 2D floor plan is shown in three areas on the right), and the body list is shown on the left. (b) Setting Field window showing the default initial source model settings.

After that, users can select one of the tools on the "Add Body" panel to create anomalous bodies. G&M3D 1.0 supports sequential creation of multiple anomaly bodies, with all generated bodies automatically listed in the "Body List" section. To ensure modelling flexibility and operational efficiency, right-click functionality is provided for existing anomalies, allowing users to modify and delete them. The modification process uses the same intuitive interface as the creation process, making it just as easy to change bodies as it is to create them. G&M3D 1.0 also allows overlapping anomalous bodies. In overlapping regions, the physical properties of the later-created body overwrite those previously assigned to the corresponding prisms.

The following section explains the construction methods for regular and irregular bodies, which differ in their modelling approaches. However, both types share the same parameter configurations for gravity and magnetic properties. As shown in the "Property" panel of Figure 6, only four parameters need to be specified: density contrast, induced magnetization intensity, magnetic declination, and magnetic inclination. Spatially heterogeneous physical-property distributions within a single body can be represented in G&M3D 1.0 through continuously varying functions. In particular, the software supports user-defined functional forms, which allow flexible construction of bodies with spatially variable density contrast or magnetization.

G&M3D 1.0 provides five tools for creating regular-shaped bodies: **Sphere**, **Cuboid**, **Cylinder**, **Ellipsoid** and **Prismoid**. Figure 6 displays the parameter input interfaces for each tool. (1) **Sphere**: This tool requires the radius and the coordinates of the sphere's center. (2) **Cuboid**: Users must input the geometric centre coordinates and the extension lengths along three orthogonal axes. (3) **Cylinder**: Four key parameters are needed to define a cylinder, including the trend direction, extension length, cross-sectional radius, and section centre coordinates. (4) **Ellipsoid:** A rotated ellipsoid is defined by the centre coordinates, the radii of the three semi-axes, and the rotation angle. (5) **Prismoid**: This geometry is defined by three sets of spatial parameters: the x-coordinates of its four y-parallel edges, the y-coordinates of its four x-parallel edges, and the z-values for its top and bottom planes. To enhance modelling flexibility, the "Direction" parameter specifies the normal vector orientation of the bounding planes relative to the coordinate axes. The **Prismoid** tool maintains strict geometric validity by enforcing essential constraints: the x-coordinates must be monotonically increasing ($x1 < x2$), and the y-coordinates ($y1 < y2$) likewise, ensuring proper spatial relationships for meaningful prism construction. All bodies require input of either density contrast or magnetization. Additionally, the "Mark" panel allows users to customize both the body's name and display colour according to their preferences. As an example, we create two bodies using each tool, resulting in a total of ten bodies, which

are presented in Figure 7.

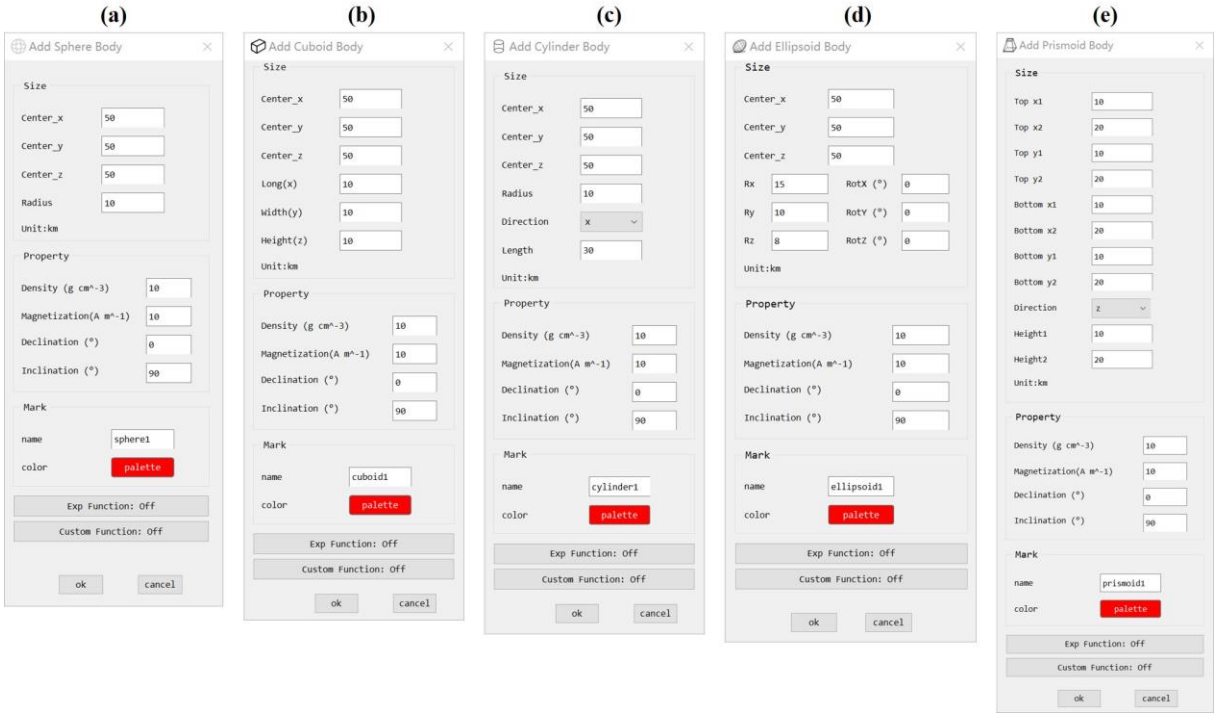

Figure 6: Parameter input interfaces for the five regular tools, including (a) Sphere, (b) Cuboid, (c) Cylinder, (d) Ellipsoid, and (e) Prismoid.

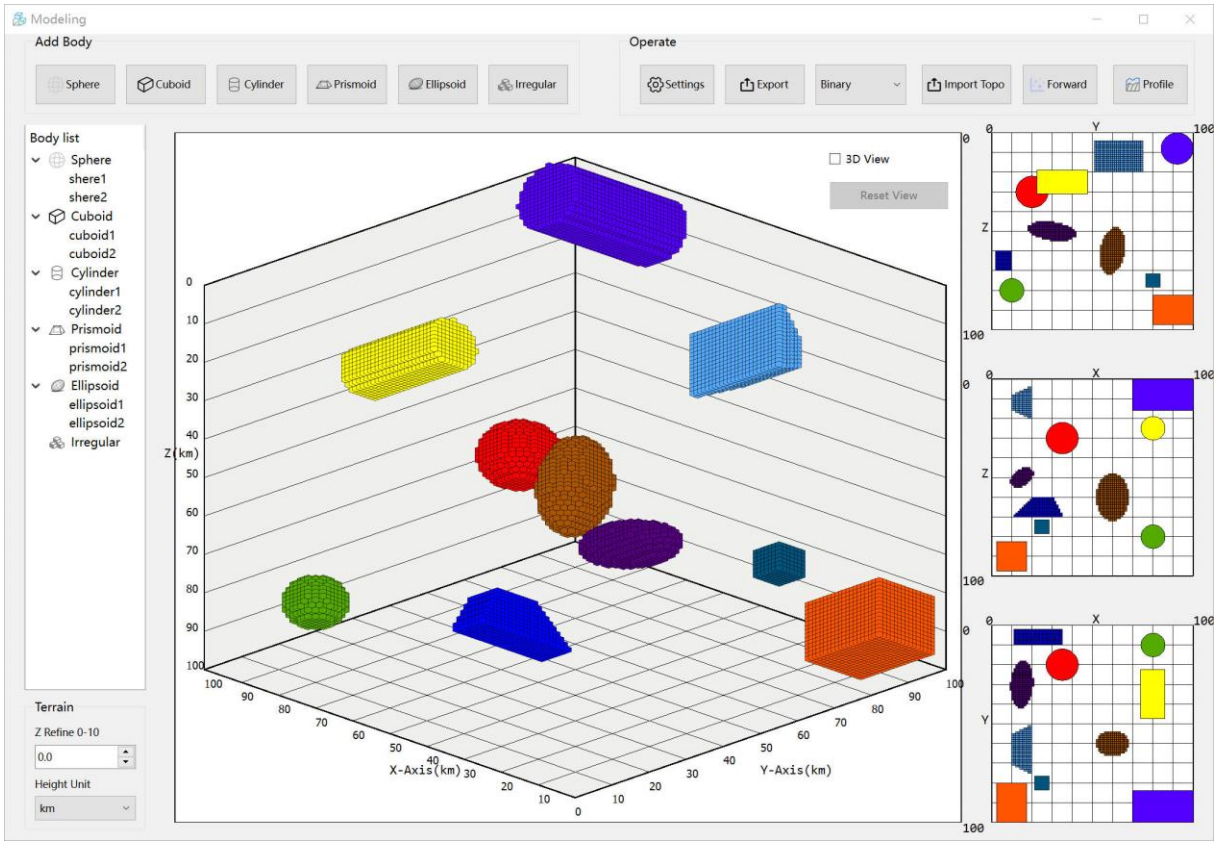

Figure 7: Illustration of regular modelling tools showing ten anomalous bodies.

G&M3D 1.0 features an **Irregular** tool that enables users to create irregular bodies, as shown in Figure 8. With the **Irregular** tool, users can accurately construct irregularly shaped bodies by interactively drawing their spatial boundaries across multiple layers. This layer-stacking method allows for the reconstruction of complex volumetric shapes that cannot be represented using conventional geometric primitives. G&M3D 1.0 automatically generates a set of prisms that fit within the limits defined by users in one layer, extending along the *x*, *y*, or *z* direction. To enhance operational efficiency, the software employs a dual-

mode: Build Mode for creating anomalous prismatic units, and Erase Mode for removing existing anomalous units. These complementary modes work in tandem to minimize operational errors, effectively eliminating the need for complete rebuilds in case of mistakes. To maximize operational flexibility while avoiding redundant constraints, both modes maintain identical workflows and interaction processes. To facilitate reference-guided modelling, the Irregular tool also allows users to load a semi-transparent background image as a visual reference (Figure 8).

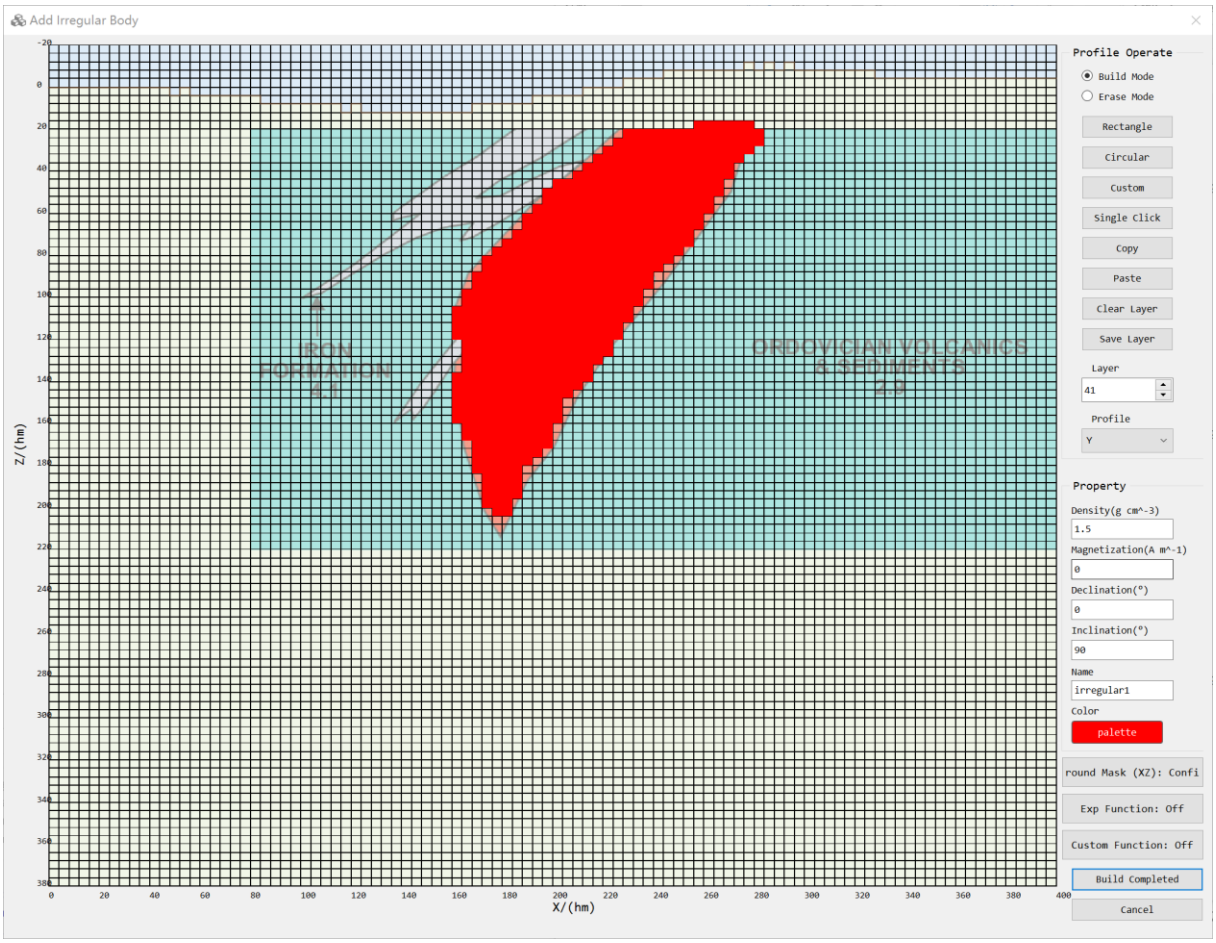

Figure 8: Interface of the Irregular tool. The main area is used to delineate the boundaries of the anomalous bodies. Right panels contain functional zones and parameter setting areas. Build Completed and Cancel buttons are used to finalize or abort the entire irregular modelling process, while all other functions only operate on the current layer. In this example, a screenshot adapted from Thomas (1997) is used as a semi-transparent background template to construct an irregular sulphide deposit with a density contrast of 1.5 g·cm^{-3}.

In the **Irregular** tool, G&M3D 1.0 offers four drawing modes: **Rectangle**, **Circular**, **Custom**, and **Single Click**. The modelling process uses a standardized left-click operation across all modes. Users press and hold the mouse button to activate a real-time visual preview of the modelling area, and release it to confirm and finalize the operation. In the **Custom** mode, users can draw any closed curve to define the boundary of the anomalous body, allowing automatically generated prisms to fit the boundaries more accurately with gradual sketching. To enhance workflow efficiency, G&M3D 1.0 includes **Copy** and **Paste** functionality for layers. Once users have finalized the geometric modelling and parameter settings (via the unified Property panel, consistent with regular modelling tools) for the current layer, they must manually save the layer data using the **Save Layer** option. After completing the model construction for all target layers, users can execute the "**Build Completed**" command to finalize and save the complete dataset. An example of constructing an irregular sulphide deposit model beneath undulating topography is shown in Figure 9.

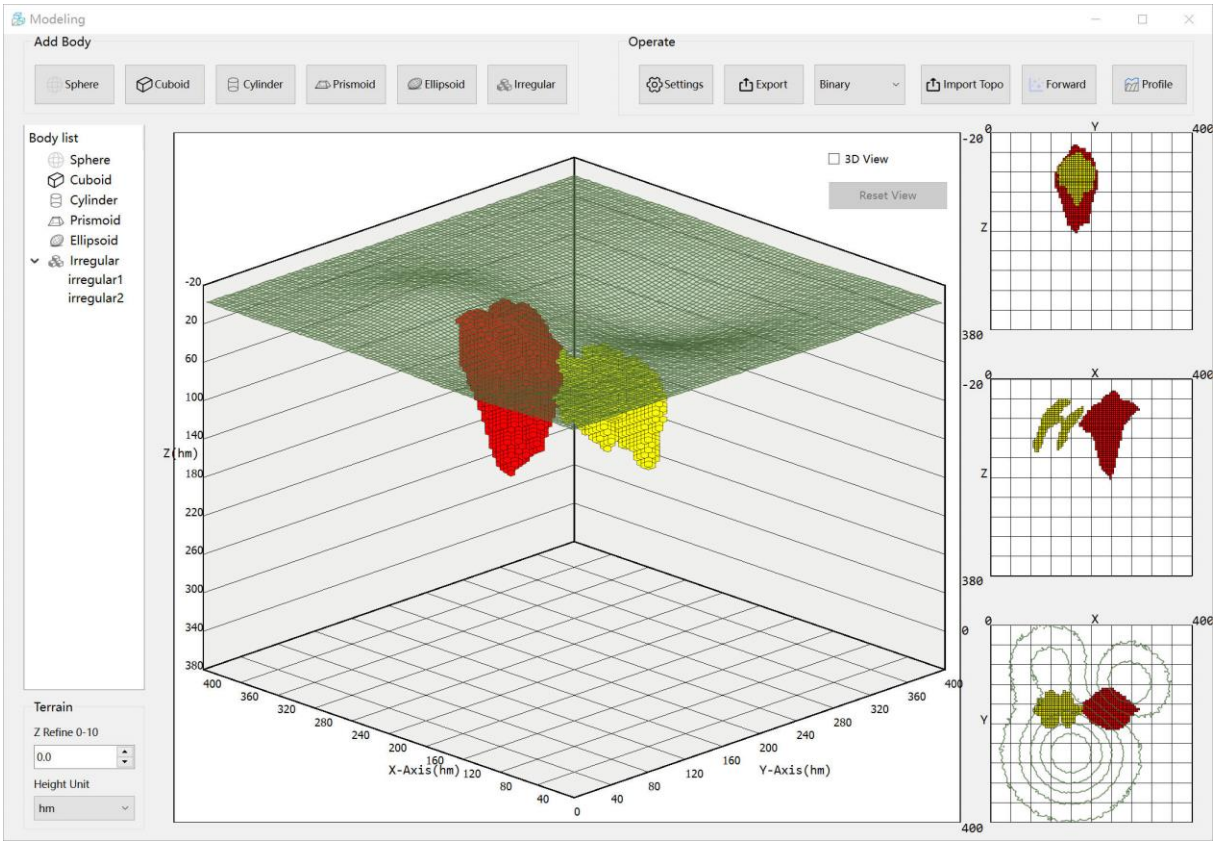

Figure 9: An irregular sulphide deposit model constructed using the Irregular tool.

Once all anomalous bodies have been constructed, G&M3D 1.0 allows users to export both the model geometry and the corresponding physical property distributions in multiple data formats. Supported export formats currently include binary, text and UBC-GIF, which can be selected directly from the drop-down menu in the **Export** tool. This design not only facilitates the segmentation of workflows between building source models and forward modelling tasks, potentially assigned to different operators, but also enhances operational flexibility throughout the gravity and magnetic data processing workflow. The binary .bin format efficiently retains comprehensive parametric data, while the text-based .txt export adheres to standardized formatting specifications to facilitate interdisciplinary data exchange.

G&M3D 1.0 provides two methods for forward modelling. Users can either initiate the computation through the **Forward** tool found in the "Operate" panel (Figure 5) to build source models and perform forward modelling within a unified project environment or directly import the pre-constructed models into the Forward-Modelling module using the **Input Model** option (Figure 4). Figure 10 shows the main interface of the Forward-Modelling module. To perform forward calculations, users must first select the desired anomalous bodies by checking the corresponding boxes in the "Body list" panel. Once the bodies are selected, users can initiate the forward modelling process by clicking the **Forward Model** button, which opens the Forward Model interface (Figure 10b). In this interface, users configure the observation parameters, including observation height and optional noise levels for simulating mobile-platform gravity and magnetic surveys. In addition, users can choose whether to enable parallel computation and whether to perform the calculation with topography. After configuring these settings, clicking the **ok** button will execute the forward calculation. Upon completion, G&M3D 1.0 automatically generates a pseudocolor plot of the results. Users can switch between different datasets using the drop-down box. The forward modelling results can be viewed in G&M3D 1.0 or exported as datasets by clicking the **Save Data** button.

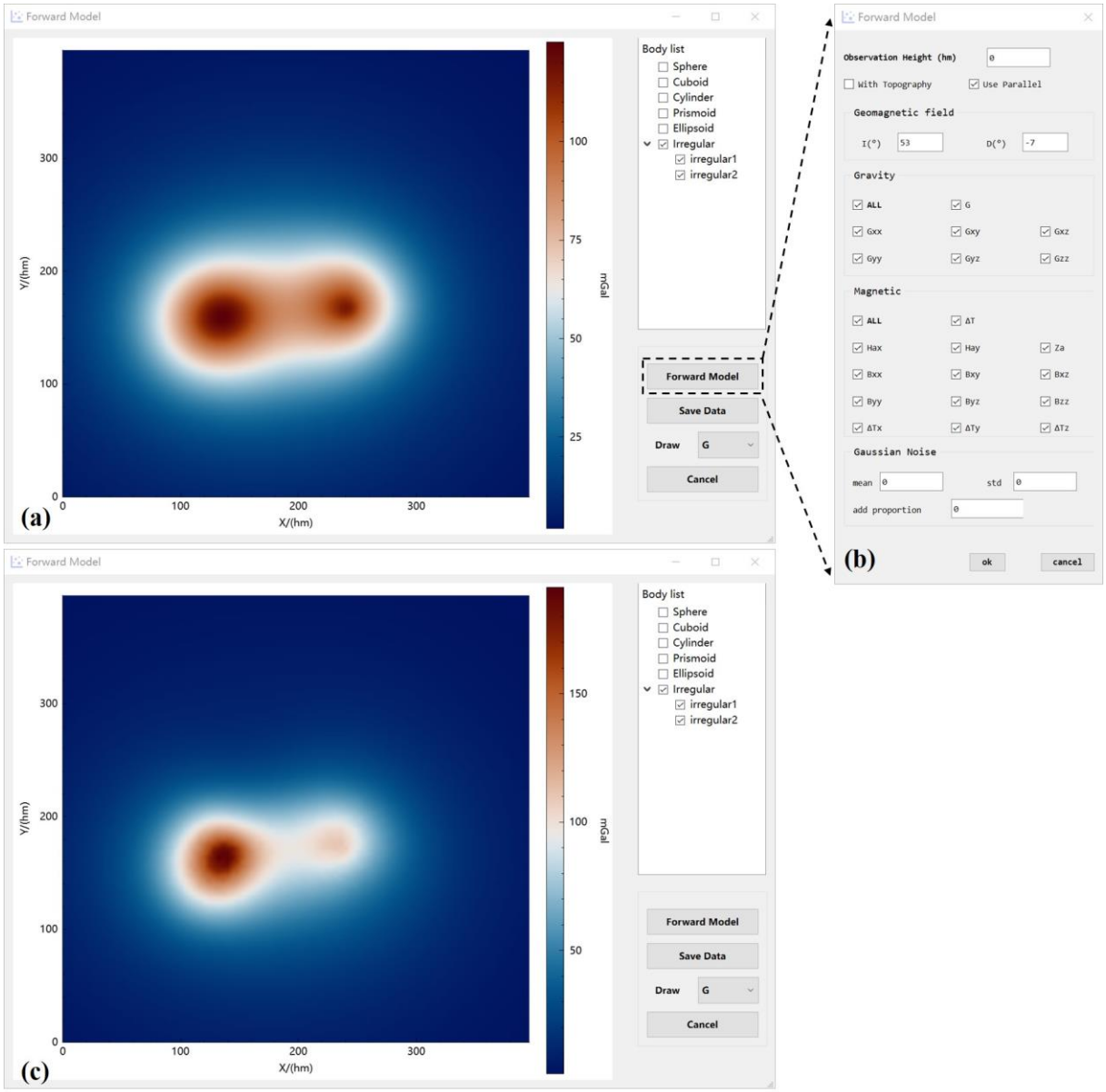

Figure 10: (a) Interface of the Forward-Modelling module. The left workspace is used to visualize the gravity/magnetic field. The upper right area shows the body list, and different bodies can be selected for forward calculation. The functional control area is located in the lower right section. A sulphide deposit is shown as an example, adapted according to Thomas (1997). (b) Parameter input pop-up window for Gravity forward modelling, Magnetic forward modelling. A certain proportion of Gaussian noise can be added to the field values to simulate errors. Mag-Inclination and Mag-Declination correspond to the inclination (I) and declination (D) of the Earth's geomagnetic field in Eqs. (17) to (20). Users can freely select the field category to be calculated. (c) Results calculated over undulating topography.

4 Application

The 3D modelling and forward calculations of the gravity and magnetic fields in G&M3D 1.0 provide practical tools for potential data analysis and interpretation. Although inversion is not implemented in the current version, the software provides flexible initial or synthetic models for studies related to inversion. Researchers often conduct synthetic model experiments to test the feasibility of their algorithms and assess parameter sensitivity. With G&M3D 1.0, they can easily create numerous density contrast or susceptibility models and quickly obtain the gravity/magnetic data. Moreover, G&M3D 1.0 serves as a practical educational resource for teaching geophysics, particularly for beginners in gravity and magnetic exploration. Educators and students can utilize G&M3D 1.0 to construct simplified geophysical models, enabling them to explore the principles of the potential fields through interactive visualization and analysis.

To illustrate the functionality of G&M3D 1.0, we perform a gravity modelling analysis of a representative salt dome as an example. This salt dome model is based on available seismic and drill-hole data from Vinton Dome in southern Louisiana

(Ennen, 2012). It features a caprock with positive-density contrast at depths ranging from 160 to 760 m, alongside a negative-density contrast salt volume located deeper. In the study by Ennen (2012), gravity gradients produced by this salt dome model are calculated and compared to observed airborne gravity gradient data to identify potential oil signals. As highlighted by Ennen (2012), constructing such an irregular density contrast model for a salt dome is a labor-intensive process.

In this example, we utilize the salt dome model described by Ennen (2012) to demonstrate the 3-D modelling and forward calculations of gravity gradients using G&M3D 1.0. According to this study, the source space is divided into 66 × 45 × 28 prisms with dimensions of 100×100×100 m. The density anomaly of the salt dome varies in geometry at different depths, with differing density contrasts, as presented in Table 2.

Table 2: Density contrast distribution of the salt dome model along the depth

Anomalous body number	Depth range of sources (m)	Density contrast (kg·m^{-3})
1	60-160	575
2	160-260	575
3	260-360	400
4	360-460	400
5	460-760	50
6	760-1060	-20
7	1060-1360	-50
8	1360-1660	-70
9	1660-1960	-100
10	1960-2260	-130
11	2260-2560	-150
12	2560-2860	-170

In G&M3D 1.0, we apply the **Irregular** tool in the Modelling Module to create a density contrast model of the salt dome. This salt dome structure can be approximated by 12 separate irregular bodies located at different depths, each with a constant density contrast, as shown in Table 2. We build these bodies successively using the Modelling Module in G&M3D 1.0. First, we set the range for the source region in the x, y, and z axes to [0 7 km], [0 7 km], and [0 5 km], respectively. The division step is set to be 100 × 100 × 100 m^3. Next, in the Layer-Building interface, we specify the layer number as 28 and the density contrast as -170 kg·m^{-3}. Using **Custom** mode, we outline the geometry of the salt dome at this depth in the workspace, and then we use **Single Click** mode to make slight modifications to its shape. After making these modifications, we save this anomalous body and change the layer number to 27. The copy and paste functions allow us to visualize the source geometry from the previous layer on the interface, which facilitates anomaly source localization. Users can easily modify the existing layer structure, significantly improving modelling efficiency. This process can be repeated to quickly build the complete salt dome model (Figure 11).

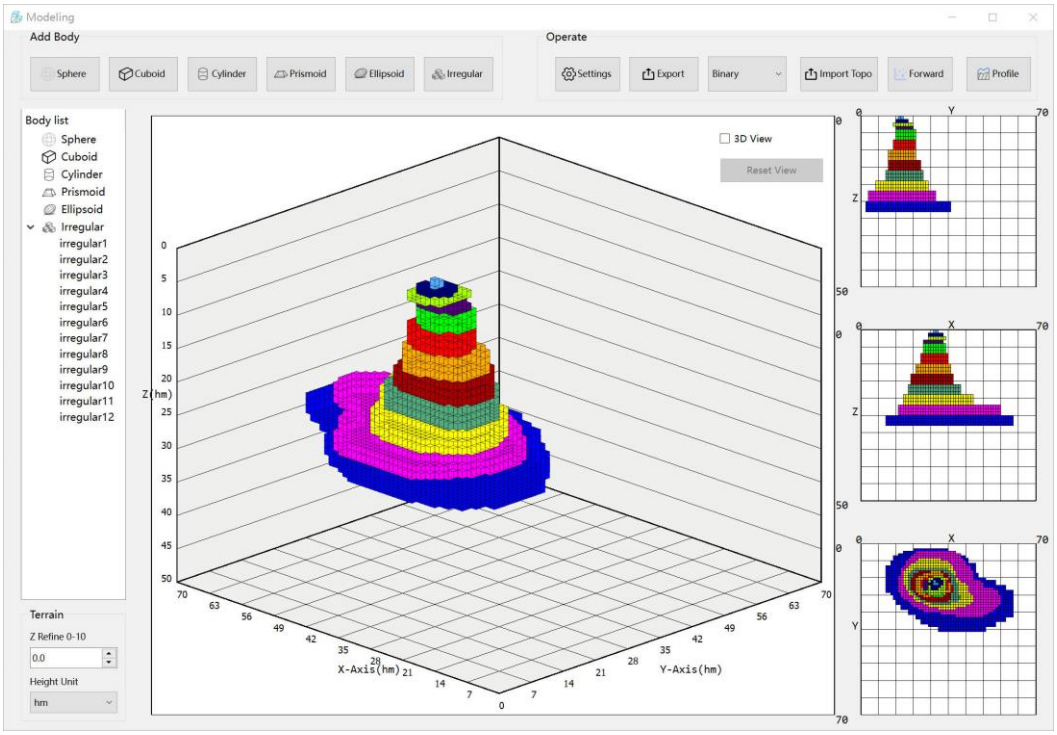

Figure 11: The salt dome model built by G&M3D 1.0.

After constructing the 12 anomalous bodies that form the salt dome model, we use the Forward Modelling Module to calculate the gravity fields and gradients. We set the observation range to match that of the source, with the observation height fixed at 200 m. The resulting gravity fields and gradient components are shown in Figure 12. To validate the accuracy of G&M3D 1.0, we conduct a comparative analysis with spatial domain approaches (Li and Chouteau, 1998). The maximum absolute difference is 1.2×10^{-12} mGal for the gravity anomaly and 1.3×10^{-12} E for the gravity-gradient components. These data are consistent with the forward simulation results provided by Ennen (2012), confirming the accuracy of the forward calculation in G&M3D 1.0.

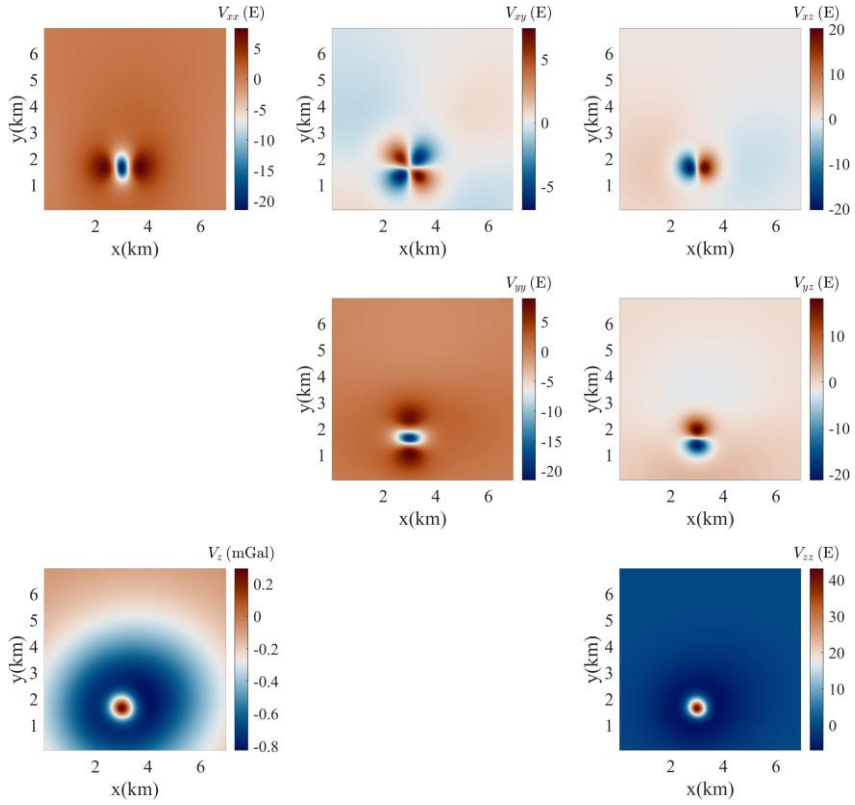

Figure 12: The gravity field and gradient components generated by the salt dome model using G&M3D 1.0. Here, 1 mGal = 10^{-5} m·s^{-2} and 1 E = 10^{-9} s^{-2}.

5 Conclusions

The study introduces an open-source software called G&M3D 1.0, developed using the Qt application framework and C++ programming language. G&M3D 1.0 is designed to create 3D models of density contrast and magnetization, as well as to compute their gravity and magnetic fields. Users can run the software either from source code or as a standalone desktop application. With G&M3D 1.0, users can easily create arbitrary anomalous bodies and perform modifications, deletions, storage, and display of the model. Furthermore, G&M3D 1.0 extends the efficient BCE algorithm for forward calculations of gravity gradient tensors and magnetic gradient tensors. Lastly, we demonstrate the gravity modelling over the Vinton salt dome in southern Louisiana, U.S. This practical application illustrates how G&M3D 1.0 can be utilized for geophysical research, training, data processing and interpretation. The modular architecture of G&M3D 1.0 also provides a robust foundation for future extensions, including incorporating additional body types, more flexible property representations, and advanced new forward functions.

Code and data availability

The G&M3D 1.0 source code used in this study is available at https://doi.org/10.5281/zenodo.17511807 (Wang et al., 2025a). The input and output data presented in this manuscript are available from https://doi.org/10.5281/zenodo.17512458 (Wang et al., 2025b).

Author contribution

Dengkang Wang: Developed the codes, and drafted the paper. Bo Chen: Provided the ideas and their implementation, and revised the paper. Kanggui Wei: Developed the codes, and drafted the paper. Jiaxiang Peng: Provided the initial functions for magnetic forward calculations. Rongwen Guo: Revised the paper.

Acknowledgments

We thank Longwei Chen and Shiyu Zhang for their help in the software development. We thank the High-Performance Computing Center of Central South University for support. The research is supported by the Deep Earth Probe and Mineral Resources Exploration - National Science and Technology Major Project (No. 2025ZD1009100) and National Natural Science Foundation of China (Grant Nos. 42474123, 42074109).

Declaration of interests

The authors declare that they have no known competing financial interests or personal relationships that could have appeared to influence the work reported in this paper.

References

Bauville, A., & Baumann, T. S., 2019. geomIO: An open-source MATLAB toolbox to create the initial configuration of 2-D/3-D thermo-mechanical simulations from 2-D vector drawings. Geochemistry, Geophysics, Geosystems, 20(3), 1665-1675. DOI: https://doi.org/10.1029/2018GC008057.

Bhattacharyya, B., 1964. Magnetic anomalies due to prism-shaped bodies with arbitrary polarization. Geophysics 29, 517-531. DOI: https://doi.org/10.1190/1.1439386.

Bhattacharyya, B., Navolio, M., 1976. A fast Fourier transform method for rapid computation of gravity and magnetic

anomalies due to arbitrary bodies. Geophys. Prospect. 24, 633-649. DOI: https://doi.org/10.1111/j.1365-2478.1976.tb01562.x.

Blakely, R.J., 1996. Potential theory in gravity and magnetic applications. Cambridge University Press. DOI: https://doi.org/10.1017/CBO9780511549816.

Caratori Tontini, F., Cocchi, L., Carmisciano, C., 2009. Rapid 3-D forward model of potential fields with application to the Palinuro Seamount magnetic anomaly (southern Tyrrhenian Sea, Italy). J. Geophys. Res. 114. DOI: https://doi.org/10.1029/2008JB005907.

Chen, L., Liu, L., 2019. Fast and accurate forward modelling of gravity field using prismatic grids. Geophys. J. Int. 216, 1062-1071. DOI: https://doi.org/10.1093/gji/ggy480.

Cockett, R., Kang, S., Heagy, L. J., Pidlisecky, A., & Oldenburg, D. W., 2015. SimPEG: An open source framework for simulation and gradient based parameter estimation in geophysical applications. Computers & Geosciences, 85, 142-154. DOI: https://doi.org/10.1016/j.cageo.2015.09.015.

de la Varga, M., Schaaf, A., Wellmann, F., 2019. GemPy 1.0: open-source stochastic geological modeling and inversion. Geoscientific Model Development 12, 1-32. DOI: https://doi.org/10.5194/gmd-12-1-2019.

Ennen, C., 2012. Mapping gas-charged fault blocks around the Vinton Salt Dome, Louisiana using gravity gradiometry data. M.S. thesis, Dept. Earth Atmos. Sci., Univ. Houston, Houston, TX, USA.

Guo, Z.H., Guan, Z.N., Xiong, S.Q., 2004. Cuboid Delta T and its gradient forward theoretical expressions without analytic odd points. Chinese Journal of Geophysics-Chinese Edition 47, 1131-1138. DOI: https://doi.org/10.1002/cjg2.615.

Hassanzadeh, A., Vázquez-Suñé, E., Corbella, M., Criollo, R., 2022. An automatic geological 3D cross-section generator: Geopropy, an open-source library. Environmental Modelling & Software 149, 105309. DOI: https://doi.org/10.1016/j.envsoft.2022.105309

Hinze, W.J., von Frese, R.R.B., Saad, A.H., 2013. Gravity and magnetic exploration: Principles, practices, and applications. Cambridge University Press. DOI: https://doi.org/10.1017/CBO9780511843129.

Hogue, J.D., Renaut, R.A., Vatankhah, S., 2020. A tutorial and open source software for the efficient evaluation of gravity and magnetic kernels. Computers & Geosciences 144, 104575. DOI: https://doi.org/10.1016/j.cageo.2020.104575.

Jessell, M., Ogarko, V., De Rose, Y., Lindsay, M., Joshi, R., Piechocka, A., Grose, L., De La Varga, M., Ailleres, L., Pirot, G., 2021. Automated geological map deconstruction for 3D model construction using map2loop 1.0 and map2model 1.0. Geoscientific Model Development 14, 5063-5092. DOI: https://doi.org/10.5194/gmd-14-5063-2021.

Li, X., Chouteau, M., 1998. Three-dimensional gravity modeling in all space. Surv. Geophys. 19, 339-368. DOI: https://doi.org/10.1023/A:1006554408567.

Luo, Y., Yao, C., 2007. Forward modeling of gravity, gravity gradients, and magnetic anomalies due to complex bodies. Journal of China University of Geosciences 18, 280-286. DOI: https://doi.org/10.1016/S1002-0705(08)60008-4.

Nagy, D., 1966. The gravitational attraction of a right rectangular prism. Geophysics 31, 362-371. DOI: https://doi.org/10.1190/1.1439779.

Nagy, D., Papp, G., Benedek, J., 2000. The gravitational potential and its derivatives for the prism. J. Geod. 74, 552-560. DOI: https://doi.org/10.1007/s001900000116.

Okabe, M., 1979. Analytical expressions for gravity anomalies due to homogeneous polyhedral bodies and translations into magnetic anomalies. Geophysics 44, 730-741. DOI: https://doi.org/10.1190/1.1440973.

Pirot, G., Joshi, R., Giraud, J., Lindsay, M.D., Jessell, M.W., 2022. loopUI-0.1: indicators to support needs and practices in 3D geological modelling uncertainty quantification. Geoscientific Model Development 15, 4689-4708. DOI: https://doi.org/10.5194/gmd-15-4689-2022.

Plouff, D., 1976. Gravity and magnetic fields of polygonal prisms and application to magnetic terrain corrections. Geophysics 41, 727-741. DOI: https://doi.org/10.1190/1.1440645.

Qiang, J., Zhang, W., Lu, K., Chen, L., Zhu, Y., Hu, S., Mao, X., 2019. A fast forward algorithm for three-dimensional magnetic

anomaly on undulating terrain. J. Appl. Geophys. 166, 33-41. DOI: https://doi.org/10.1016/j.jappgeo.2019.04.009.

Snopek, K., & Casten, U. 2006. 3GRAINS: 3D Gravity Interpretation Software and its application to density modeling of the Hellenic subduction zone. Computers & geosciences, 32(5), 592-603. DOI: https://doi.org/10.1016/j.cageo.2005.08.008.

Thomas, M., 1997. Gravity Prospecting For Massive Sulphide Deposits in the Bathurst Mining Camp, New Brunswick, Canada, pp. 837-840.

Ulug, R., & Karslıoglu, M. O., 2022. SRBF_Soft: a Python-based open-source software for regional gravity field modeling using spherical radial basis functions based on the data-adaptive network design methodology. Earth Science Informatics, 15(2), 1341-1353. DOI: https://doi.org/10.1007/s12145-022-00790-y.

Vogel, C.R., 2002. Computational methods for inverse problems. SIAM. DOI: https://doi.org/10.1137/1.9780898717570.

Wang, D., Chen, B., Wei, K., Peng, J., Guo, R. 2025a. GM3D-1.0, Zenodo, https://doi.org/10.5281/zenodo.17511807.

Wang, D., Chen, B., Wei, K., Peng, J., Guo, R. 2025b. G&M3D 1.0: an Interactive Framework for 3D Model Construction and Forward Calculation of Potential Fields [Data set], Zenodo, https://doi.org/10.5281/zenodo.17512458.

Wellmann, J.F., Thiele, S.T., Lindsay, M.D., Jessell, M.W., 2016. pynoddy 1.0: an experimental platform for automated 3-D kinematic and potential field modelling. Geoscientific Model Development 9, 1019-1035. DOI: https://doi.org/10.5194/gmd-9-1019-2016.

Wu, L.Y., Tian, G., 2014. High-precision Fourier forward modeling of potential fields. Geophysics 79, G59-G68. DOI: https://doi.org/10.1190/geo2014-0039.1.

Yuan, Y., Cui, Y., Chen, B., Zhao, G., Liu, J., Guo, R., 2022. Fast and high accuracy 3D magnetic anomaly forward modeling based on BTTB matrix. Chinese Journal of Geophysics-Chinese Edition 65, 1107-1124. DOI: https://doi.org/10.6038/cjg2022P0126.

Zhang, Y., Wong, Y.S., 2015. BTTB-based numerical schemes for three-dimensional gravity field inversion. Geophys. J. Int. 203, 243-256. DOI: https://doi.org/10.1093/gji/ggv301.

Zhao, G., Chen, B., Chen, L., Liu, J., Ren, Z., 2018. High-accuracy 3D Fourier forward modeling of gravity field based on the Gauss-FFT technique. J. Appl. Geophys. 150, 294-303. DOI: https://doi.org/10.1016/j.jappgeo.2018.01.002.